NSRRC - Jo 4800 (2015)

Macromolecules

Article

pubs.acs.org/Macromolecules

Evolution of Crystal Orientation in One-Dimensionally Confined Space Templated by Lamellae-Forming Block Copolymers

Chien-Liang Liu,[†] Ming-Champ Lin,*[,‡] Hsin-Lung Chen,*[,†] and Alejandro J. Müller[§,∥]

[†]Department of Chemical Engineering and Frontier Center of Fundamental and Applied Sciences of Matters, National Tsing Hua University, Hsin-Chu 30013, Taiwan

[‡]R&D Department, Chang Chun Petrochemical Co. Ltd., Miaoli 36053, Taiwan

[§]POLYMAT and Polymer Science and Technology Department, Faculty of Chemistry, University of the Basque Country UPV/EHU, Paseo Manuel de Lardizabal 3, 20018 Donostia-San Sebastián, Spain

[∥]IKERBASQUE, Basque Foundation for Science, Bilbao, Spain

Supporting Information

ABSTRACT: Polymer crystallites may exhibit preferred orientation when the crystallization is allowed to occur under the influence of spatial confinement. Using time-resolved wide-angle X-ray scattering (WAXS), we explore the time evolution of the preferred crystal orientation within one-dimensionally confined space constructed by the lamellar microdomains of two crystalline block copolymers, polyethylene-*block*-poly(DL-lactide) (PE-*b*-PDLLA) and poly(L-lactide)-*block*-polyethylene (PLLA-*b*-PE), where the developments of the parallel and the perpendicular orientation of PE and PLLA crystallites, respectively, were monitored from the early stage of crystallization. Both types of crystallites were randomly oriented at the early stage of formation. As crystallization proceeded further, the ensemble-average orientation progressively improved toward the preferred orientation type, and the rate of establishing the orientation exhibited the same dependence on crystallization temperature (T_c) as the crystallization kinetics. Further examination of the effectiveness of enhancing the average orientation with respect to the increase of crystallinity supported the postulate that the perpendicular orientation of PLLA crystallites arises from the tendency to attain long-range crystal growth, while the parallel crystal orientation of PE is driven by the excluded volume interaction between the crystallites as a result of the intrinsically high nucleating power of PE.

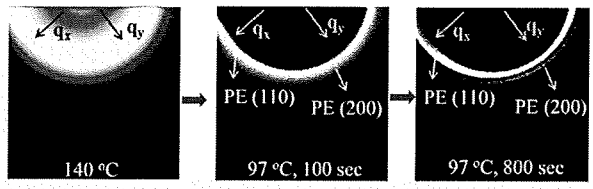

INTRODUCTION

The precise control of crystal orientation provides a methodology for directional manipulation of the properties of crystalline polymers.[1−3] The use of nanoscale templates to spatially confine the crystallization process is an effective approach to create crystal orientation over a large length scale. A number of inorganic and organic nanotemplates with distinct shapes and sizes have been employed for this purpose.[4,5] The most popular one is perhaps the nanoscale microdomains of strongly segregated block copolymers (bcps). It is known that the microphase separation between the incompatible constituting chains in bcps can generate a variety of well-defined microdomains, including lamellae, cylinders, and spheres.[6] When these domain structures are formed by the crystalline block in the melt state, they may impose the spatial confinement with different dimensionalities to the subsequent crystallization process upon cooling.

The lamellar microdomain of bcps represents the simplest confined geometry that offers one-dimensional (1-D) confinement to the crystallization process. Several factors have been identified to govern the crystal orientation in the lamellae-forming bcps, where the orientation is usually represented by the alignment of the crystalline stems (i.e., the crystallographic *c*-axis) with respect to the lamellar interface. Cheng et al. have investigated the orientation of PEO crystallites in the lamellar domains in poly(ethylene oxide)-*block*-polystyrene (PEO-*b*-PS), which is a crystalline−amorphous (C−A) system composed of a crystalline PEO block and an amorphous PS block.[7−9] It was found that the preferred orientation of the PEO stems exhibited a transformation from parallel to tilt to perpendicular type with increasing crystallization temperature (T_c).

A similar transformation of the PEO crystal orientation with increasing T_c had also been identified in a defect-free single crystal made of PEO-*b*-PS.[10−12] In contrast to that observed in the defect-containing diblock, the change of crystal orientation showed an abrupt transition from parallel to perpendicular type without the intervention of the tilt orientation. The transition temperature was shown to be governed by the confinement size and the reduced tethering density.[11,12]

Received: April 29, 2015
Revised: June 8, 2015
Published: June 29, 2015

ACS Publications © 2015 American Chemical Society

DOI: 10.1021/acs.macromol.5b00898
Macromolecules 2015, 48, 4451−4460

Table 1. Molecular Characteristics and Thermal Properties of PE-*b*-PDLLA and PLLA-*b*-PE Studied

		PLA			PE	
	PLA/PE vol fraction	$\bar{M}_n$, kg mol^{-1}	T_m, °C	T_g, °C	$\bar{M}_n$, kg mol^{-1}	T_m, °C
PE-*b*-PDLLA	47/53	32.4	N/A	55	27.7	103.5
PLLA-*b*-PE	43/57	22.5	171.7	62.1	26.5	104.2

Sun et al. have studied the crystal orientation in a series of pol(ε-caprolactone)-*block*-poly(4-vinylpyridine) (PCL-*b*-P4VP) diblock copolymers with different thicknesses of the PCL lamellar domains in the melt state.[13,14] It was demonstrated that the confinement size prescribed by the domain thickness could strongly influence the crystallization mechanism and crystal orientation; that is, decreasing the confinement size not only altered the nucleation from heterogeneous to homogeneous mechanism but also led to a transformation of PCL crystal orientation from perpendicular to parallel and even to random configuration.

Previous studies have revealed that perpendicular orientation of the crystallites with respect to the lamellar microdomain interface was prevalent among C−A diblock copolymers under typical crystallization conditions, which was consistent with simulation results.[15] However, the orientation of PE-containing C−A systems behaved anomalously, as the PE crystallites always tended to show parallel orientation.[16−18] To explore this issue, we have critically examined the orientation behavior of PE crystallites over a broad range of T_c in lamellae-forming polyethylene-*block*-poly(DL-lactide) (PE-*b*-PDLLA) diblock copolymers.[19] It was found that the orientation of PE crystallites transformed from random to parallel type with increasing T_c, while perpendicular orientation was still inaccessible even at very high T_c (ca. 2 K below the nominal melting point). We further proposed that the crystal orientation was governed by the interplay between the nucleation rate and the crystal growth kinetics, and the parallel crystal orientation predominantly observed among PE-based bcps was attributed to the excellent nucleating power of PE block.

In addition to the C−A diblock copolymers, the crystal orientation behavior in lamellae-forming bcps composed of two crystallizable blocks (i.e., the crystalline−crystalline (C−C) diblock) has also been investigated.[20−22] For this type of system, the crystalline morphology is governed by the interplay between the crystallization of the leading-crystallizing component (i.e., the component that crystallizes first) and the melt structure prescribed by microphase separation, in the same sense as that established in C−A system. As the later-crystallizing block crystallizes subsequently, its crystallization process is effectively confined within the domain structure established by the leading-crystallizing component. Although the involvement of an additional crystalline block may increase the complexity of the crystallization process, it was reported that the crystal orientation behavior in the C−C system was essentially identical to that found in C−A diblock as long as the crystallization event took place under strong confinement.[22]

Previous works exploring the crystal orientation in confined space have focused on resolving the type of orientation attained after the completion of crystallization.[7−14,16−29] In these cases, the crystallization temperature, reduced tethering density, and confinement size were found to affect the ultimate crystal orientation, as has been described above.[7−9,11−14] The evolution of crystal orientation during isothermal crystallization, which is important for understanding the mechanism of establishing the preferred orientation, has not been explored in detail thus far. It remains largely unclear how the crystallites start to develop a preferred orientation from the early stage of their formation. To resolve this issue, here we undertake time-resolved wide-angle X-ray scattering (WAXS) experiment with synchrotron radiation source to resolve the ensemble-average crystal orientation as a function of time during the crystallization process. We focus on the crystallization under the 1-D confinement established by the lamellar microdomains in a PE-*b*-PDLLA and a PLLA-*b*-PE, where PE and PLLA crystallites tend to display parallel and perpendicular orientation with respect to lamellar interface, respectively.[19,22] We will show that both types of crystallites were randomly oriented on average at the early stage of their formation. As the crystallization proceeded further, the ensemble-average orientation progressively transformed to the preferred type. A phenomenological model assuming that the refinement of the average orientation followed a first-order kinetics was formulated to describe the observed temporal development of crystal orientation. It will further be shown that the observed evolutions of crystal orientation support our previous postulate that the prevalently observed perpendicular crystal orientation arises from the tendency to attain long-range crystal growth, while the parallel crystal orientation of PE is driven by the excluded volume interaction between the crystallites due to the high nucleating power of PE.[19] Our results and analysis shall shed light on the mechanism of establishing the preferred crystal orientation under spatial confinement, which is important for expanding the window for controlling or creating new properties of semicrystalline polymers.

EXPERIMENTAL SECTION

Materials. The syntheses and characterizations of PE-*b*-PDLLA and PLLA-*b*-PE studied here have been described in previous publications.[30,31] In brief, 1,3- butadiene was anionically polymerized in cyclohexane using *sec*-butyllithium as the initiator and end-capped with ethylene oxide to form hydroxyl-terminated 1,4-polybutadiene containing ca. 93% of the 1,4-regioisomer. This polybutadiene was then hydrogenated to give hydroxyl-terminated polyethylene, which was used in combination with $AlEt_3$ as a macroinitiator in the ring-opening polymerization of DL-lactide (PDLLA) or L-lactide (PLLA). The detailed compositions and thermal properties of these two copolymers are summarized in Table 1.[32]

Bulk Sample Preparation. The films of the copolymer samples used in this study were prepared by dissolving the polymer powders in toluene at 65 °C followed by casting onto a Petri dish. The concentration of the copolymers in the solution was 5% (w/v). The solvent was then evaporated slowly at 70 °C, followed by further drying at the same temperature in vacuum for 2 days to remove the residual solvent.

Large-Amplitude Oscillatory Shear (LAOS) Experiment. LAOS was performed to produce large-scale alignment of the lamellar microdomains in PE-*b*-PDLLA and PLLA-*b*-PE. The samples were subjected to shear treatment before conducting time-resolved WAXS experiment. The samples with size of 5.0 × 5.0 × 0.2 mm^3 were placed in a Linkam CSS450 shear hot stage under a nitrogen atmosphere and were subjected to LAOS at the prescribed temperature for 2 h under oscillatory mode with a shear frequency of 0.3 Hz and strain amplitude of 70%. The operation temperatures of LAOS for PE-*b*-PDLLA and

DOI: 10.1021/acs.macromol.5b00898
Macromolecules 2015, 48, 4451−4460

PLLA-*b*-PE were 140 and 150 °C, respectively, which can lead to good alignment of lamellar microdomains. After LAOS treatment, specimens were cut into rectangular shape for X-ray scattering experiments. The 2-D small-angle X-ray scattering (SAXS) patterns (to be presented in Figures 2g and 3g) revealed that the lamellar domains in the sheared sample were macroscopically aligned with the lamellar normal directed perpendicularly to the film surface,[19,22] as schematically illustrated in Figure 1.

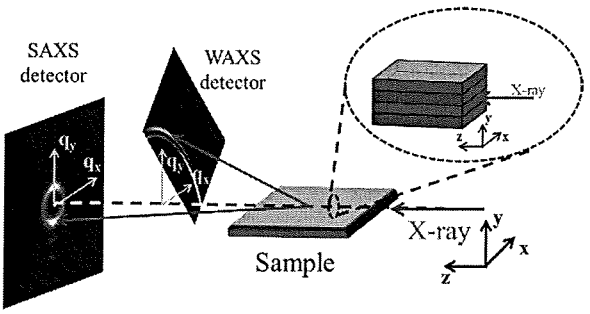

Figure 1. Schematic illustration of the configuration of the SWAXS instrument. The incident X-ray beam passes through the edge of sample. The WAXS detector plane is normal to the incident beam but tilts 45° from the *x*-axis.

X-ray Scattering Experiments. The evolution of the crystal orientation at a given T_c was examined by time-resolved WAXS experiment conducted at BL23A SWAXS beamline of the National Synchrotron Radiation Research Center (NSRRC) located at Hsinchu, Taiwan.[33] The configuration of the instrument is schematically illustrated in Figure 1. The energy of X-ray source was 15 keV (λ = 0.083 nm). A two-dimensional Mar CCD detector (512 × 512 pixel resolution) at the sample-to-detector distance of 2259 mm was used to record the 2-D SAXS scattering pattern, and a CMOS flat panel X-ray detector (C9728DK with the area of 52.8 mm^2) at the sample-to-detector distance of 124.53 mm was employed to record the 2-D WAXS scattering pattern. The WAXS detector plane was normal to the incident beam, but tilted 45° from the *x*-axis (see Figure 1). The size of the WAXS detector covered the scattering vector ($q = (4\pi/\lambda)\sin(\theta/2)$ with θ being the scattering angle) range of 4−32 nm^{-1} and the azimuthal angle range of 0−90°. The time required for collecting each WAXS pattern was 5 s. The WAXS angular scale was calibrated using silver behenate, sodalite, silicon powders, and high-density polyethylene.

Shear-oriented specimens were used to conduct the time-resolved WAXS experiments. The samples of PE-*b*-PDLLA and PLLA-*b*-PE were first annealed in the melt state at 140 °C ($>T_m^{PE}$) and 200 °C ($>T_m^{PLLA}$), respectively, for 5 min to erase the previous thermal history followed by rapid cooling to the desired T_c to allow PE and PLLA crystallization. The 2-D WAXS patterns along the edge view of the films (by having the incident X-ray traveling along the shear plane) were collected to monitor the evolution of crystal orientation during the crystallization process.

RESULTS AND DISCUSSION

Time-Resolved 2-D WAXS Patterns during Isothermal Crystallization. The hierarchical structure and the ultimate crystal orientation of the PE-*b*-PDLLA and the PLLA-*b*-PE studied here have been resolved in our previous works.[19,22] Both bcps exhibited lamellar morphology in the melt state due to their symmetric compositions. The crystallizations of both PE and PLLA blocks were effectively confined within their respective microdomains regardless of the crystallization condition because of the strong segregation between PLA and PE. Whenever a preferred orientational order was attained, parallel orientation with the crystalline stems oriented parallel to the lamellar interface was observed for PE crystallites in both copolymers, while the PLLA crystallites always adopted perpendicular orientation with the crystalline stems aligning perpendicularly to the lamellar interface in PLLA-*b*-PE, as schematically illustrated in Figures 2h and 3h. In this work, we mainly focus on the temporal development of the orientational order of PE and PLLA crystallites in PE-*b*-PDLLA and PLLA-*b*-PE, respectively, to examine the mechanism of establishing the two distinct types of orientation during isothermal crystallization.

The development of PE crystal orientation in PE-*b*-PDLLA was investigated at two crystallization temperatures (i.e., T_c = 95 and 97 °C), where the 2-D WAXS patterns were collected *in situ* with the time interval of 5 s during the crystallization process. Figure 2 shows the representative edge-view 2-D WAXS and SAXS patterns of PE-*b*-PDLLA during crystallization at the T_c indicated. The (00*l*) diffractions of the lamellar microdomains were located in the meridian direction

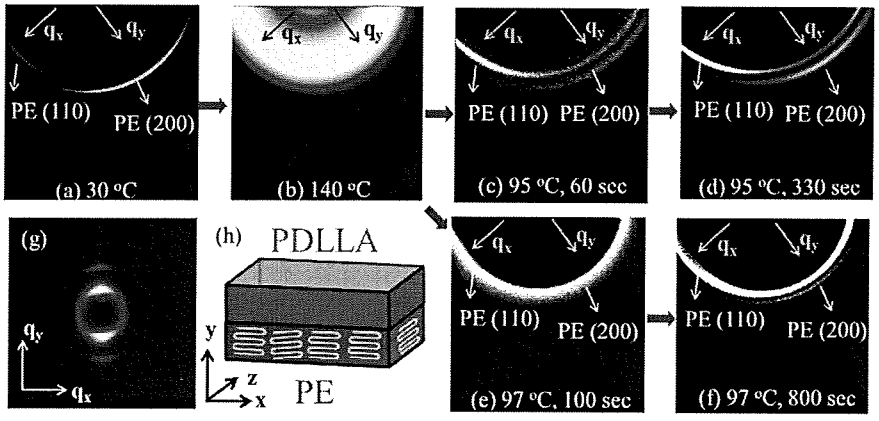

Figure 2. Representative 2-D WAXS patterns of the shear-oriented PE-*b*-PDLLA after isothermal crystallization at 95 and 97 °C for the time periods indicated. The sample obtained after the LAOS treatment (a) was melted at 140 °C (b) followed by cooling to 95 °C (c, d) or 97 °C (e, f) to induce PE crystallization. The corresponding 2-D SAXS pattern is displayed in (g) and (h) schematically illustrates the parallel orientation of PE crystallites in the lamellar microdomain.

DOI: 10.1021/acs.macromol.5b00898
Macromolecules 2015, 48, 4451−4460

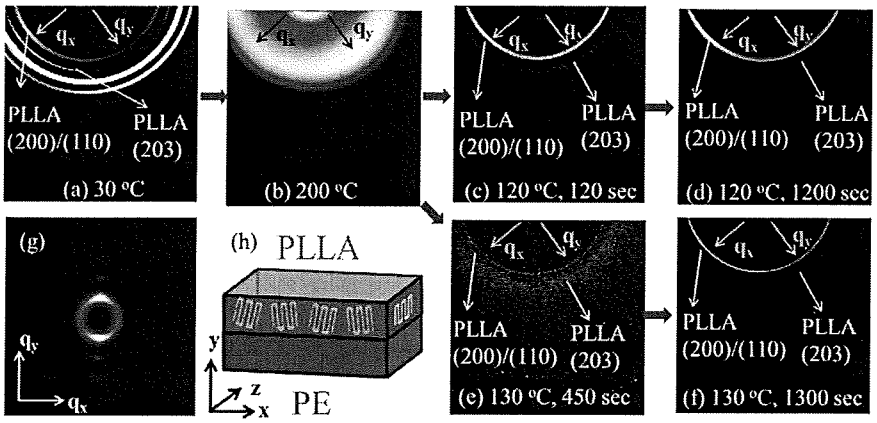

Figure 3. Representative 2-D WAXS patterns of the shear-oriented PLLA-*b*-PE after isothermal crystallization at 120 and 130 °C for the time periods indicated. The sample obtained after the LAOS treatment (a) was melted at 200 °C (b) followed by cooling to 120 °C (c, d) or 130 °C (e, f) to induce PLLA crystallization. The corresponding 2-D SAXS pattern is displayed in (g) and (h) schematically illustrates the perpendicular orientation of PLLA crystallites in the lamellar micordomain.

in the 2-D SAXS pattern (Figure 2g), indicating that the normal of the lamellar interface aligned perpendicularly to the film surface, as schematically illustrated in Figure 1. Because of the relatively small area of the WAXS detector employed, the observed WAXS pattern only covered a limited range of azimuthal angle (ϕ = 0–90°); however, the scattering pattern was sufficient for quantitatively characterizing the crystal orientation. As shown in Figure 2a, an anisotropic diffraction pattern was observed for the sample crystallized by slow cooling to 30 °C after the LAOS treatment. The inner and outer diffraction arcs are associated with the (110) and (200) diffractions of PE crystallites, respectively. The features of the diffraction pattern, with the (200) diffraction locating at the q_y direction and the angle between (110) and (200) in the azimuthal scan being 56.3°, were consistent with the previously reported results showing that the PE crystallites adopted parallel orientation (cf. Figure 2h).[19]

Upon heating to 140 °C (a temperature of ca. 35 °C higher than the nominal melting point of PE block), an amorphous halo was identified in the WAXS pattern (cf. Figure 2b), signaling that the PE was in the molten state. When the system was subsequently cooled to 95 °C for isothermal crystallization, the crystallization of PE blocks started to take place at 30 s (to be shown later in Figure 6a). In this case, the (110) and (200) diffractions appeared as arcs in the WAXS pattern collected at the beginning of crystallization ($t \cong 60$ s), as shown in Figure 2c, indicating that the preferred crystal orientation has already developed early. Such a preferred orientation became more obvious with increasing crystallization time (cf. Figure 2d). The results in Figure 2c,d thus revealed that the parallel orientation of PE crystallites was attained at the early stage of crystallization at 95 °C, and this type of orientation conserved until the end of crystallization.

In order to reveal if the preferred crystal orientation always appeared at the onset of crystallization, the crystallization of PE block at a higher T_c of 97 °C (with slower crystallization rate) was examined. The onset of crystallization at this T_c was delayed to 50 s (to be shown later in Figure 6b), and the features of the corresponding WAXS pattern at the beginning of crystallization were different from those observed at 95 °C. As in the case of Figure 2e, the crystal diffractions were essentially isotropic when the crystallization just took place ($t \cong$ 100 s). The isotropic rings transformed to anisotropic arcs as the crystallization progressed (cf. Figure 2f), and this anisotropic pattern persisted to the final state. The results thus demonstrated that PE crystallites were randomly oriented at the early stage of crystallization, but they adjusted toward the preferred orientation as the crystallization proceeded further.

Figure 3 displays the representative edge-view 2-D WAXS and SAXS patterns of PLLA-*b*-PE for examining the orientation of PLLA crystallites during isothermal crystallization in the lamellar microdomain. The diblock was annealed first at 200 °C ($> T_m^{PLLA} > T_m^{PE}$), followed by cooling to the desired T_c ($T_m^{PE} < T_c < T_m^{PLLA}$) to allow isothermal crystallization of PLLA. The 2-D SAXS pattern shown in Figure 3g also showed that the normal of the lamellar microdomains was perpendicular to the film surface. For the sample cooled after the LAOS treatment, the two inner diffraction arcs shown in Figure 3a are associated with the (110)/(200) and (203) diffractions of PLLA crystallites. The fact that the (200) diffraction was along the q_x direction, which agreed with our previous study, indicated that the *a*-axis of the PLLA unit cell was parallel with respect to the lamellar interface and hence the crystallographic *c*-axis or the crystalline stem was perpendicular to the interface.[22]

The as-crystallized sample was subsequently heated to 200 °C to completely melt the PLLA and PE crystallites (as evidenced in Figure 3b showing that the crystalline diffractions of PLLA and PE completely vanished and the WAXS pattern contained only the isotropic amorphous halos) followed by prompt cooling to T_c to induce PLLA crystallization. It was found that the preferred orientation of PLLA crystallites developed at the very early stage of crystallization at the lower T_c of 120 °C (see Figure 3c and Figure S1), and such a preferred orientation persisted until the end of crystallization (cf. Figure 3d and Figure S1). On the other hand, at the higher T_c of 130 °C the crystallites were randomly oriented at the beginning of crystallization (cf. Figure 3e), but the originally isotropic WAXS rings transformed to anisotropic arcs as the crystallization occurred further, signaling that the randomly oriented PLLA crystallites adjusted to the perpendicular orientation (see Figure 3f).

The 2-D WAXS patterns in Figures 2 and 3 offered a first glance at the time evolution of the orientational order of PE and PLLA crystallites formed within the lamellar micro-

DOI: 10.1021/acs.macromol.5b00898
Macromolecules 2015, 48, 4451–4460

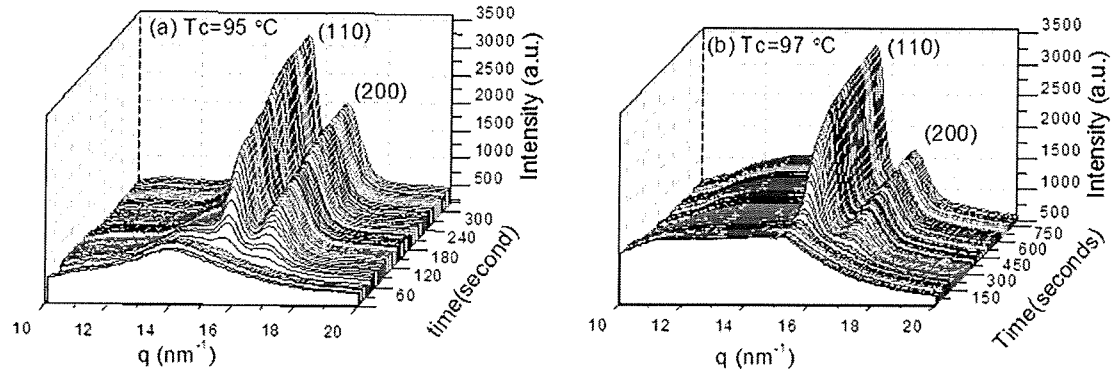

Figure 4. Time-resolved 1-D WAXS intensity profiles of PDLLA-*b*-PE with the PE block subjecting to isothermal crystallization at (a) 95 °C and (b) 97 °C.

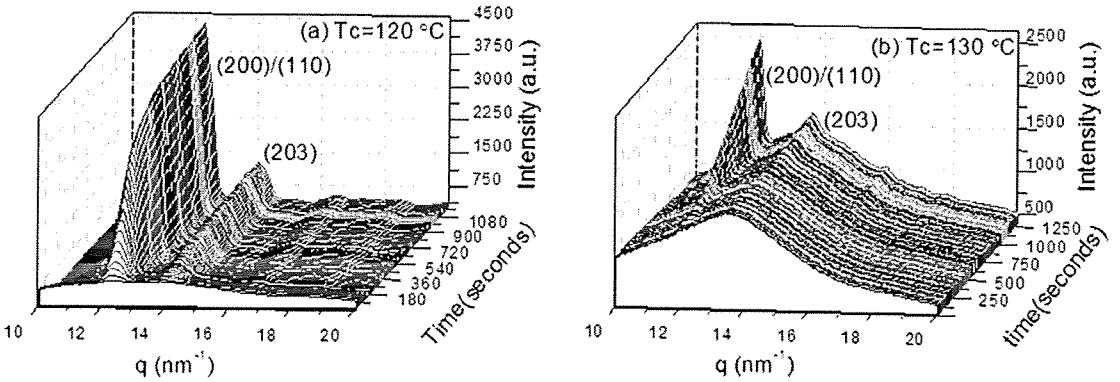

Figure 5. Time-resolved 1-D WAXS intensity profiles of PLLA-*b*-PE with the PLLA block subjecting to isothermal crystallization at (a) 120 °C and (b) 130 °C.

domains. Both crystallites were randomly oriented on average at the beginning of crystallization, but they adjusted toward their preferred orientations as the crystallization proceeded. The time duration over which the random orientation existed was shorter under faster crystallization (i.e., at lower T_c).

The time-resolved WAXS 1-D intensity profiles of PE-*b*-PDLLA and PLLA-*b*-PE subjected to the isothermal crystallizations are displayed in Figures 4 and 5, respectively. Figures 4a and 4b show the results of PE-*b*-PDLLA in which the PE block was allowed to crystallize at 95 and 97 °C, respectively. The peaks at q = 15.2 and 16.8 nm^{-1} are associated with the (110) and (200) diffractions of PE crystallites, respectively. At 95 °C, these diffraction peaks emerged at 30 s followed by obvious increases of their intensities with crystallization time. Similar results were found for T_c = 97 °C, except that the appearance of the diffraction peaks was delayed to 50 s, and the crystallinity attained at the end of the WAXS measurement (t = 800 s) was lower than that observed at 95 °C, due to slower crystallization at the lower degree of undercooling.

The time-resolved WAXS intensity profiles for the crystallization of PLLA block in PLLA-*b*-PE at T_c = 120 and 130 °C are shown in Figures 5a and 5b, respectively. It can be seen from Figure 5a that the crystallization of PLLA block occurred as soon as the system was brought to 120 °C, as evidenced by the immediate appearance of the diffraction peaks at 11.7 and 13.3 nm^{-1}, which correspond to the (110)/(200) and (203) diffractions of PLLA crystallites, respectively. The crystallinity then gradually increased and approached saturation by 800 s. The crystallization of PLLA block was significantly slower at 130 °C, where the crystallinity was essentially undetectable until 175 s has elapsed (see Figure 5b). In this case, the crystallinity still kept growing even after 1300 s. The time-resolved 1-D intensity profiles as well as the corresponding 2-D patterns were further analyzed to obtain the time evolutions of crystallinity and crystal orientation function, respectively. The results are to be presented in the following section.

Time Evolutions of Crystallinity and Crystal Orientation Function. The WAXS profiles in Figures 4 and 5 were employed to calculate the degree of crystallinity X_c as a function of time during the crystallization process via $X_c = A_c/(A_c + A_a)$, with A_c and A_a being the areas of the crystal diffraction peaks and the amorphous halo, respectively. The deconvolution of the peaks in the WAXS profiles was performed with the PeakFit v4.11 software, assuming Gaussian function for each peak.

The crystal orientation can be presented quantitatively by the orientation function (f) calculated using the intensity distributions along the azimuthal angle (ϕ) of (200) and (110)/(200) diffractions of PE and PLLA crystallites, respectively, in the 2-D patterns. Since the WAXS patterns collected here did not cover the entire range of the azimuthal scan, we adopted the equation derived by Higa et al.,[20] which allows the orientation function to be calculated from the range of azimuthal angles from 0 to 90°. The ensemble-average orientation function of the crystallites is given by

DOI: 10.1021/acs.macromol.5b00898
Macromolecules 2015, 48, 4451−4460

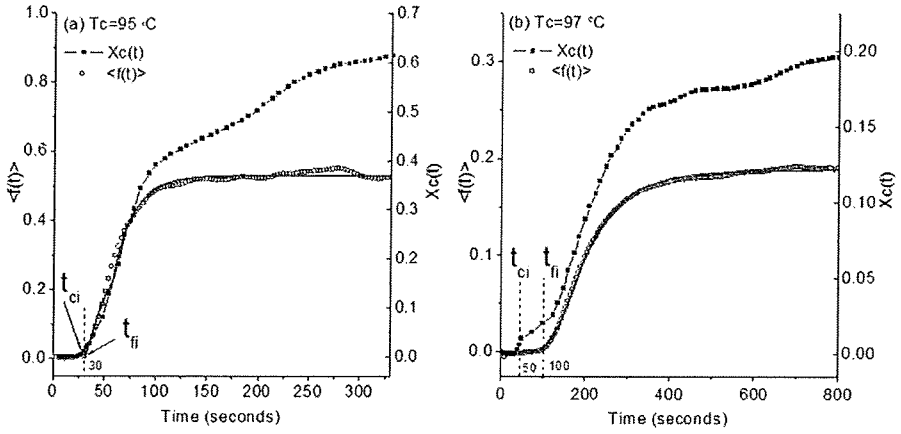

Figure 6. Time evolutions of the ensemble-average orientation function $\langle f(t)\rangle$ and crystallinity $X_c(t)$ of PE blocks in PE-*b*-PDLLA in the isothermal crystallization at (a) 95 °C and (b) 97 °C. t_{ci} and t_{fi} signfy the induction time of crystallization and orientation development, respectively. The red curves represent the fits by the phenomological model based on eqs 4 and 5.

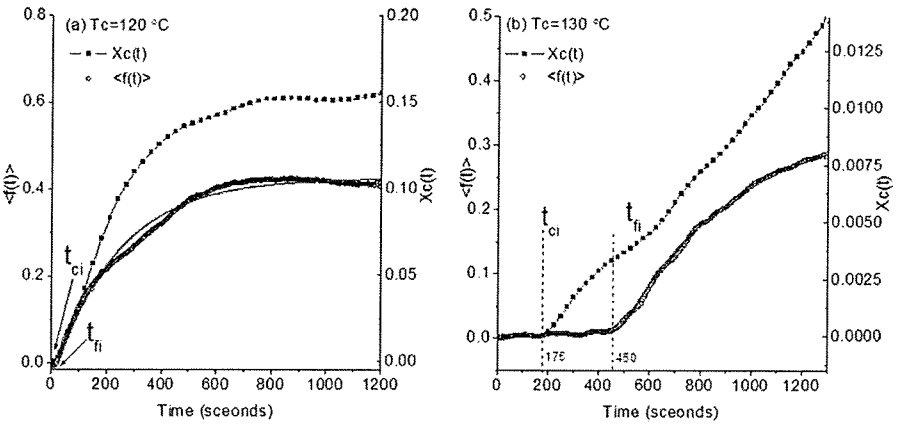

Figure 7. Time evolutions of the ensemble-average orientation function $\langle f(t)\rangle$ and crystallinity $X_c(t)$ of PLLA blocks in PLLA-*b*-PE in the isothermal crystallization at (a) 120 °C and (b) 130 °C. t_{ci} and t_{fi} signfy the induction time of crystallization and orientation development, respectively. The red curves represent the fits by the phenomological model based on eqs 4 and 5.

$$\langle f\rangle = \frac{k^{-1}\langle\cos^2\phi\rangle - 1}{k^{-1} - 1} \tag{1}$$

where k represents the value of $\langle\cos^2\phi\rangle$ at random orientation. For the calculation of $\langle\cos^2\phi\rangle$, we adopted the following equation reported by Higa et al.

$$\langle\cos^2\phi\rangle = \frac{\int_0^{\pi/2} I(\phi)\cos^2(\phi-\sigma)|\sin(\phi-\sigma)|\,d\phi}{\int_0^{\pi/2} I(\phi)|\sin(\phi-\sigma)|\,d\phi} \tag{2}$$

where $I(\phi)$ is the azimuthal intensity distribution for a specific diffraction and σ is the azimuthal angle at which the maximum intensity is located in the azimuthal scan range. $\langle f\rangle$ calculated from eqs 1 and 2 has a value of 1 when the normal of the diffraction plane is perfectly parallel to the reference direction located at $\phi = \sigma$; a value of 0 indicates that the diffraction intensity is equally distributed around ϕ, and hence the crystallites are randomly oriented. Thus, a larger value of $\langle f\rangle$ signifies the higher degree of crystal orientation in a specific type (i.e., parallel or perpendicular).

Figures 6a and 6b show the temporal variations of $X_c(t)$ and $\langle f(t)\rangle$ of PE crystallites in PE-*b*-PDLLA during isothermal crystallization at T_c = 95 and 97 °C, respectively. As the system reached 95 °C upon cooling from the melt, the crystallization of PE blocks started to take place at ca. 30 s, and the crystallinity increased abruptly up to ca. 100 s. The preferred crystal orientation developed almost as soon as the crystallization started, and the orientation function increased concomitantly with the crystallinity development over the time interval of 30 s < t < 100 s. However, the orientation function reached the ultimate value after ca. 135 s, whereas the crystallinity still continued to develop until ca. 290 s.

To resolve if the crystallites started to develop the preferred orientation at the onset of crystallization, the time evolutions of $X_c(t)$ and $\langle f(t)\rangle$ associated with the slower PE crystallization at a higher temperature (T_c = 97 °C) were examined (see Figure 6b). It can be seen from Figure 6b that between 50 and 100 s the crystallinity grew obviously with time; however, the corresponding value of $\langle f(t)\rangle$ remained at nearly zero. The result demonstrates that the average orientation of PE crystallites was essentially random at the early stage of crystallization. The value of $\langle f(t)\rangle$ increased progressively with time as the crystallinity developed further at 100 s $\leq t \leq$ 475 s, signaling that a significant fraction of PE crystallites

DOI: 10.1021/acs.macromol.5b00898
Macromolecules 2015, 48, 4451−4460

started to align toward the parallel orientation. The orientation function was also found to reach the ultimate value before the completion of crystallization at this T_c.

In order to understand if the characteristics of the temporal evolution of crystal orientation observed above are universal, we further probed the development of the perpendicular orientation of PLLA crystallites during the isothermal crystallization in PLLA-*b*-PE. Figures 7a and 7b display the $X_c(t)$ and $\langle f(t)\rangle$ of PLLA as a function of time at T_c = 120 and 130 °C, respectively. The crystallization started as soon as the temperature reached 120 °C; in this case, the values of $\langle f(t)\rangle$ and $X_c(t)$ increased concomitantly with time (Figure 7a). The observed features of the developments of crystallinity and orientation function were analogous to those found for PE crystallization in PE-*b*-PDLLA at 95 °C (i.e., the crystallization at the higher undercooling). When the PLLA-*b*-PE was subjected to crystallization at the higher T_c of 130 °C, the results in Figure 7b clearly revealed that the development of PLLA crystallinity occurred prior to that of $\langle f(t)\rangle$ at the early stage of crystallization ($t \leq 450$ s). Because the crystallization rate was slow, both the average orientation function and crystallinity have not reached their ultimate values at the end of the experiment (t = 1300 s). Therefore, similar to that found for PE crystallites formed at the higher T_c, the PLLA crystallites were randomly oriented on average at the early stage of crystallization; they started to align toward the perpendicular orientation after an induction time (denoted as t_{fi}).

Our time-resolved WAXS results have demonstrated that the features of the crystal orientation development were universal irrespective of the type of orientation attained ultimately. The ensemble-average orientation of the crystallites formed at the early stage of crystallization was random; after a certain induction time, the average orientation function started to increase from zero value, signaling that a significant fraction of the crystallites began to align toward the preferred orientation. In the case of PE, the orientation function reached the ultimate value before the completion of the crystallization process. Moreover, the rate of the development of crystal orientation was in accord with the crystallization kinetics, where the crystallites started to align toward the preferred orientation and reached the ultimate orientation earlier at the lower T_c where the crystallization was faster.

Proposed Model for the Time Evolution of Crystal Orientation. The fact that the rate of the development of orientational order exhibited the same temperature dependence as the crystallization kinetics supports our previous postulate that the preferred crystal orientation attained in the confined space is kinetically driven.[19] When a given crystallite just forms in the lamellar microdomain, it does not tend to adopt a preferred orientation since its size is too small to feel the spatial confinement. In this case, its initial orientation with respective to the lamellar interface is arbitrary. As the crystallite grows to a significant size where its growth front is near the lamellar interface, the boundary set by the interface may frustrate further crystal growth. In order to continue the growth process effectively, the crystallite should attempt aligning its crystalline stems perpendicularly to the interface, because such a perpendicular orientation is the most kinetically favorable in the sense that it allows not only the long-range growth along the direction of the lamellar interface but also the effective surface spreading of the crystalline stems along the lateral direction of the crystallite, which is an elementary step in crystal growth.[34] The orientational order of the crystallite is expected to improve progressively during crystal growth; as a result, the rate of the development of perpendicular crystal orientation exhibits the same temperature dependence as the crystal growth rate.

For PE, the parallel crystal orientation was attributed to its good nucleating power,[19] where a large number of crystallites may form in a given microdomain within a short time interval, leading to dense crystallite population in the domain. In this case, a given crystallite may experience strong excluded volume interaction with the neighboring crystallites when two of them are sufficiently close. It is known that the excluded volume interaction between the discotic liquid crystalline molecules can give rise to regular stacking of the dislike molecules to form a columnar mesophase.[35] Such a scenario should also apply to the crystallites which is lamellae in shape; consequently, once the excluded volume interaction between the growing crystallites is strong, it would drive the crystallites (with the crystalline stems aligning normal to the basal surface of the crystallite) to stack along the direction of lamellar domain interface, which then yields the parallel crystal orientation. The establishment of such a parallel crystal orientation is hence expected to be more rapid under a faster nucleation.

The orientation function measured at a given time by WAXS is not associated with a single crystallite but instead represents the ensemble average of the orientation of all crystallites present at that time. Here we formulate a phenomenological model to quantitatively fit the observed temporal evolution of the ensemble-average crystal orientation functions displayed in Figures 6 and 7. In the time-resolved WAXS experiment, each scattering pattern was collected at the time interval of Δt = 5 s. We designate the crystallites developed over each time interval as a "group". The ensemble-average orientation function calculated at time t, $\langle f(t)\rangle$, which is given by the average over the orientation functions of all crystallites present at time t, can also be obtained by averaging the "group-average orientation functions" of all groups having been developed as of time t, namely

$$\langle f(t)\rangle = \frac{\sum_{i=1}^{N_c(t)} f_i(t)}{N_c(t)} = \frac{\sum_{j=1}^{N_g(t)} \langle f_{gj}(t)\rangle}{N_g(t)} \tag{3}$$

where $f_i(t)$ is the orientation function of the individual crystallites at time t, $N_c(t)$ is the total number of crystallites present at time t, $N_g(t)$ is the number of groups having been developed as of time t, and $\langle f_{gj}(t)\rangle$ is the group-average orientation function of group j given by $\langle f_{gj}(t)\rangle = (\sum_{i=1}^{N_{gc}} f_{ji}(t))/N_{gc}$, with N_{gc} being the number of crystallites per group which may be expressed as $N_{gc} = I\Delta t$ (I = nucleation rate prescribing the number of nuclei developed per unit time) and $f_{ji}(t)$ being the orientation function of crystallite i in group j.

When a given group of crystallites just form in the lamellar microdomains, they do not tend to adopt the preferred orientation since their sizes are too small to feel the spatial confinement, as has been discussed above. In this case, the group-average orientation function $\langle f_{gj}(t)\rangle$ of the arbitrarily oriented crystallites is zero at the early stage of formation for all groups. This random orientation persists over an induction time t_{fi}, after which the crystallites start to adjust toward the preferred orientation. Therefore, $\langle f_{gj}(t)\rangle$ increases progressively with time after the induction period. For group j formed at time τ_j, the crystallites belonging to this group have already taken the time of $(t - \tau_j - t_{fi})$ in adjusting their orientation. We assume

DOI: 10.1021/acs.macromol.5b00898
Macromolecules 2015, 48, 4451−4460

that the kinetics of the adjustment of orientation follows the following exponential function

$$\langle f_{gj}(t)\rangle = f_\infty(1 - e^{-k(t-\tau_j-t_{fi})}) \quad \text{for } (t-\tau_j) > t_{fi} \tag{4}$$

and

$$\langle f_{gj}(t)\rangle = 0 \quad \text{for } (t-\tau_j) > t_{fi} \tag{5}$$

where f_∞ is the ultimate value of the orientation function and k is the rate constant associated with the adjustment of orientation. Equation 4 was derived from the first-order kinetics equation, which postulates that the rate of adjusting the orientational order decreases progressively as the ultimate value f_∞ is approached due to decrease of driving force. By recognizing that $\tau_j = j\Delta t$ and $N_g(t) = t/\Delta t$, the ensemble-average orientation function $\langle f(t)\rangle$ was calculated from eqs 3 to 5 as a function of time. The calculated curves are displayed along with the experimental data in Figures 6 and 7. It can be seen that the model adopted fitted the experimental results fairly well. The values of the rate constant and induction time obtained from the fitting are listed in Table 2.

Table 2. Values of the Rate Constant and Induction Time Obtained from the Fittings of the Observed Time Evolutions of $\langle f(t)\rangle$ in Figures 6 and 7 Using the Phenomenological Model Based on Eqs 4 and 5

sample	T_c (°C)	rate constant, k (1/s)	induction time, t_{fi} (s)
PE-*b*-PDLLA	95	4.93×10^{-2}	2
	97	1.15×10^{-2}	85
PLLA-*b*-PE	120	4.30×10^{-3}	0
	130	2.23×10^{-3}	255

It is interesting to note that at the end of the time-resolved WAXS experiment the crystallinity of PLLA attained at 130 °C ($X_c = 0.013$) was much lower than that attained at 120 °C ($X_c = 0.15$), as shown in Figure 7b; however, the ensemble-average orientation function reached at 130 °C ($\langle f\rangle = 0.27$) was not much smaller than that achieved at 120 °C ($\langle f\rangle = 0.4$). This observation implies that the development of the perpendicular orientation of PLLA during the crystallization at 130 °C was far more effective than that at 120 °C.

Figure 8 plots the ensemble-average orientation as a function of crystallinity for both PE and PLLA to demonstrate the effect described above more clearly. Comparing to the crystallization at 120 °C, the orientation function of PLLA increased much more abruptly with increasing crystallinity at 130 °C. The opposite was however observed for PE, where the increase of crystal orientation function with the development of crystallinity at 97 °C was less steep than that at 95 °C. As long as the crystallization kinetics is controlled by the thermodynamic driving force, the increase of T_c (or the decrease of the degree of undercooling, ΔT) would slow down the nucleation rate (I) more than the crystal growth rate (G), since I and G vary with the undercooling via $I \sim \exp(-1/\Delta T^2)$ and $G \sim \exp(-1/\Delta T)$. At 130 °C we may envision that the nucleation of PLLA was so slow that only a minor fraction of the PLLA microdomains contained the crystallites or each lamellar microdomain contained a very small number of crystallites. These crystallites, although grew more slowly at the higher T_c, may improve their orientation toward the perpendicular configuration effectively because there was essentially no interference from other crystallites in the domain during the growth; consequently, the relatively high ensemble-average orientation may be attained at low overall crystallinity of PLLA. The observation that the perpendicular crystal orientation develops much more effectively at the higher T_c further supports our postulate that the attainment of such an orientation is governed by the crystal growth.

On the other hand, the parallel orientation of PE crystallites is driven by the excluded volume interaction due to its high nucleating power. The establishment of such an orientational order should be effective when the nucleation rate takes place efficiently relative to the crystal growth. As has been indicated, increasing T_c depresses the nucleation rate more than the growth rate; as a result, the rate of establishing the parallel orientation with respect to the increase of crystallinity becomes slower at the higher T_c. In the case where the nucleation density in the sample reached saturation, the ensemble average of the parallel orientation may also reach an ultimate value, but the development of crystallinity still continues by crystal growth. As a result, $\langle f(t)\rangle$ of PE reached the saturated level before the completion of crystallization, as found in Figure 6.

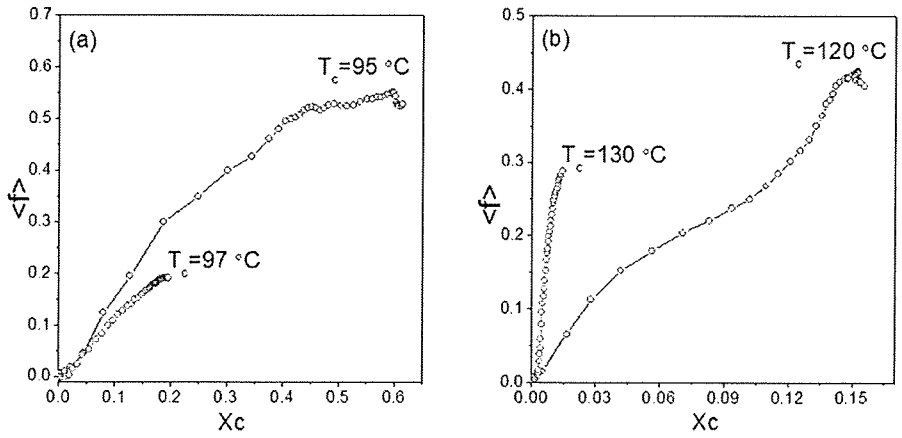

Figure 8. Enhancement of the ensemble-average crystal orientation with respect to the increase of crystallinity in the isothermal crystallization of (a) PE-*b*-PDLLA and (b) PLLA-*b*-PE. The crystallization temperatures are indicated in the figures.

DOI: 10.1021/acs.macromol.5b00898
Macromolecules 2015, 48, 4451−4460

CONCLUSIONS

The time evolution of crystal orientation in 1-D confined space templated by the lamellar microdomains of block copolymer has been resolved by time-resolved WAXS technique, where the development of parallel and perpendicular orientation of PE and PLLA crystallites in lamellae-forming PE-*b*-PDLLA and PLLA-*b*-PE, respectively, was monitored from the beginning of the crystallization. Both types of crystallite were randomly oriented on average at the early stage of crystallization. They progressively adjusted their orientation toward the preferred type after an induction time, and the time evolution of the orientational order was described satisfactorily by a first-order kinetics. The random orientation at the early stage of crystallization was attributed to the fact that the crystallite size was too small to experience the spatial restriction to crystal growth set by the interface of the lamellar microdomains. When the PLLA crystallites grew to a significant size, they started to adjust their orientation to attain long-range growth by aligning the crystalline stems perpendicularly to the interface of the lamellar microdomain. In the case of PE, a dense population of crystallite population may form in the microdomain within a short time period due to its good nucleating power; in this case, the strong excluded volume interaction between the crystallites gave rise to the parallel crystal orientation. The key roles of crystal growth and nucleation on the attainment of perpendicular and parallel orientation, respectively, were supported by examining the effectiveness of establishing the orientational order with respect to the increase of crystallinity.

ASSOCIATED CONTENT

Supporting Information

The 2D WAXS patterns of Figures 3c and 3d with modified contrast to demonstrate the difference in polarization of the (110)/(200) reflections between the crystallization time of 120 and 1200 s for PLLA block in PLLA-*b*-PE crystallized at 120 °C; the azimuthal scans of the intensity of (110)/(200) reflections in the 2D WAXS patterns of Figures 3c and 3d. The Supporting Information is available free of charge on the ACS Publications website at DOI: 10.1021/acs.macromol.5b00898.

AUTHOR INFORMATION

Corresponding Authors

*E-mail hlchen@che.nthu.edu.tw (H.-L.C.).
*E-mail mingchamp@msn.com (M.-C.L.).

Notes

The authors declare no competing financial interest.

ACKNOWLEDGMENTS

This work is supported by the Ministry of Science of Technology under Grants MOST 103-2221-E-007-133 and MOST 103-2622-E-007-025.

REFERENCES

(1) Chen, D.; Zhao, W.; Russell, T. P. *ACS Nano* **2012**, *6* (2), 1479–1485.
(2) Wu, Y.; Gu, Q.; Ding, G.; Tong, F.; Hu, Z.; Jonas, A. M. *ACS Macro Lett.* **2013**, *2* (6), 535–538.
(3) Wang, H.; Keum, J. K.; Hiltner, A.; Baer, E. *Macromolecules* **2009**, *42* (18), 7055–7066.
(4) Carr, J. M.; Langhe, D. S.; Ponting, M. T.; Hiltner, A.; Baer, E. *J. Mater. Res.* **2012**, *27* (10), 1326–1350.
(5) Lin, M.-C.; Nandan, B.; Chen, H.-L. *Soft Matter* **2012**, *8* (28), 7306–7322.
(6) Khandpur, A. K.; Forster, S.; Bates, F. S.; Hamley, I. W.; Ryan, A. J.; Bras, W.; Almdal, K.; Mortensen, K. *Macromolecules* **1995**, *28* (26), 8796–8806.
(7) Huang, P.; Zhu, L.; Guo, Y.; Ge, Q.; Jing, A. J.; Chen, W. Y.; Quirk, R. P.; Cheng, S. Z. D.; Thomas, E. L.; Lotz, B.; Hsiao, B. S.; Avila-Orta, C. A.; Sics, I. *Macromolecules* **2004**, *37* (10), 3689–3698.
(8) Zhu, L.; Calhoun, B. H.; Ge, Q.; Quirk, R. P.; Cheng, S. Z. D.; Thomas, E. L.; Hsiao, B. S.; Yeh, F.; Liu, L.; Lotz, B. *Macromolecules* **2001**, *34* (5), 1244–1251.
(9) Zhu, L.; Cheng, S. Z. D.; Calhoun, B. H.; Ge, Q.; Quirk, R. P.; Thomas, E. L.; S, H. B. *J. Am. Chem. Soc.* **2000**, *122* (25), 5957–5967.
(10) Hsiao, M.-S.; Chen, W. Y.; Zheng, J. X.; Van Horn, R. M.; Quirk, R. P.; Ivanov, D. A.; Thomas, E. L.; Lotz, B.; Cheng, S. Z. D. *Macromolecules* **2008**, *41* (13), 4794–4801.
(11) Hsiao, M.-S.; Zheng, J. X.; Leng, S.; Van Horn, R. M.; Quirk, R. P.; Thomas, E. L.; Chen, H.-L.; Hsiao, B. S.; Rong, L.; Lotz, B.; Cheng, S. Z. D. *Macromolecules* **2008**, *41* (21), 8114–8123.
(12) Hsiao, M.-S.; Zheng, J. X.; Horn, R. M. V.; Quirk, R. P.; Thomas, E. L.; Chen, H.-L.; Lotz, B.; Cheng, S. Z. D. *Macromolecules* **2009**, *42* (21), 8343–8352.
(13) Sun, Y.-S.; Chung, T.-M.; Li, Y.-J.; Ho, R.-M.; Ko, B.-T.; Jeng, U.-S. *Macromolecules* **2007**, *40* (18), 6778–6781.
(14) Sun, Y.-S.; Chung, T.-M.; Li, Y.-J.; Ho, R.-M.; Ko, B.-T.; Jeng, U.-S.; Lotz, B. *Macromolecules* **2006**, *39* (17), 5782–5788.
(15) Hu, W. *Macromolecules* **2005**, *38* (9), 3977–3983.
(16) Kofinas, P.; Cohen, R. E. *Macromolecules* **1994**, *27* (11), 3002–3008.
(17) Hamley, I. W.; Fairclough, J. P. A.; Ryan, A. J.; Bates, F. S.; Towns-Andrews, E. *Polymer* **1996**, *37* (19), 4425–4429.
(18) Hamley, I. W.; Fairclough, J. P. A.; Terrill, N. J.; Ryan, A. J.; Lipic, P. M.; Bates, F. S.; TownsAndrews, E. *Macromolecules* **1996**, *29* (27), 8835–8843.
(19) Lin, M.-C.; Wang, Y.-C.; Chen, H.-L.; Müller, A. J.; Su, C.-J.; Jeng, U.-S. *J. Phys. Chem. B* **2011**, *115* (11), 2494–2502.
(20) Higa, T.; Nagakura, H.; Sakurai, T.; Nojima, S. *Polymer* **2010**, *51* (23), 5576–5584.
(21) Lu, S.; Yuxiu, L.; Lei, Z.; S, H. B.; A, A.-O. C. *Polymer* **2004**, *45* (24), 8181–8193.
(22) Lin, M.-C.; Wang, Y.-C.; Chen, J.-H.; Chen, H.-L.; M Ller, A. J.; Su, C.-J.; Jeng, U.-S. *Macromolecules* **2011**, *44* (17), 6875–6884.
(23) Douzinas, K. C.; Cohen, R. E. *Macromolecules* **1992**, *25* (19), 5030–5035.
(24) Nakagawa, S.; Kadena, K.-i.; Ishizone, T.; Nojima, S.; Shimizu, T.; Yamaguchi, K.; Nakahama, S. *Macromolecules* **2012**, *45* (4), 1892–1900.
(25) Huang, P.; Guo, Y.; Quirk, R. P.; Ruan, J.; Lotz, B.; Thomas, E. L.; Hsiao, B. S.; Avila-Orta, C. A.; Sics, I.; Cheng, S. Z. D. *Polymer* **2006**, *47* (15), 5457–5466.
(26) Huang, P.; Zhu, L.; Cheng, S. Z. D.; Ge, Q.; Quirk, R. P.; Thomas, E. L.; Lotz, B.; Hsiao, B. S.; Liu, L.; Yeh, F. *Macromolecules* **2001**, *34* (19), 6649–6657.
(27) Huang, P.; Zheng, J. X.; Leng, S.; Van Horn, R. M.; Jeong, K.-U.; Guo, Y.; Quirk, R. P.; Cheng, S. Z. D.; Lotz, B.; Thomas, E. L.; Hsiao, B. S. *Macromolecules* **2007**, *40* (3), 526–534.
(28) Zhu, L.; Mimnaugh, B. R.; Ge, Q.; Quirk, R. P.; Cheng, S. Z. D.; Thomas, E. L.; Lotz, B.; Hsiao, B. S.; Yeh, F.; Liu, L. *Polymer* **2001**, *42* (21), 9121–9131.
(29) Ho, R.-M.; Lin, F.-H.; Tsai, C.-C.; Lin, C.-C.; Ko, B.-T.; Hsiao, B. S.; Sics, I. *Macromolecules* **2004**, *37* (15), 5985–5994.
(30) Anderson, K. S.; Hillmyer, M. A. *Polymer* **2004**, *45* (26), 8809–8823.
(31) Wang, Y.; Hillmyer, M. A. *J. Polym. Sci., Part A: Polym. Chem.* **2001**, *39* (16), 2755–2766.
(32) Castillo, R. V.; Müller, A. J.; Lin, M.-C.; Chen, H.-L.; Jeng, U.-S.; Hillmyer, M. A. *Macromolecules* **2008**, *41* (16), 6154–6164.
(33) Jeng, U.-S.; Su, C. H.; Su, C.-J.; Liao, K.-F.; Chuang, W.-T.; Lai, Y.-H.; Chang, J.-W.; Chen, Y.-J.; Huang, Y.-S.; Lee, M.-T.; Yu, K.-L.; Lin, J.-M.; Liu, D.-G.; Chang, C.-F.; Liu, C.-Y.; Chang, C.-H.; Liang, K. S. *J. Appl. Crystallogr.* **2010**, *43*, 110–121.

DOI: 10.1021/acs.macromol.5b00898
Macromolecules 2015, 48, 4451–4460

(34) Hoffman, J. D.; Davis, G. T.; Lauritzen, J. I. The Rate of Crystallization of Linear Polymers with Chain Folding. In *Treatise on Solid State Chemistry*; Hannay, N. B., Ed.; Plenum Press: New York, 1976; Vol. 3, Chapter 7, pp 497−614.
(35) Jones, R. A. L. *Soft Condensed Matter*; Oxford University Press: Oxford, 2002.

DOI: 10.1021/acs.macromol.5b00898
Macromolecules 2015, 48, 4451−4460